Locally Low-Rank Tensor Regularization for High-Resolution Quantitative Dynamic MRI

Burhaneddin Yaman, Sebastian Weingärtner, Nikolaos Kargas, Nicholas D. Sidiropoulos and Mehmet Akçakaya
Department of Electrical and Computer Engineering
University of Minnesota, Minneapolis, MN
Emails: {yaman013, sweingae, karga005, sidir001, akcakaya}@umn.edu

***Abstract*—Quantitative dynamic MRI acquisitions have the potential to diagnose diffuse diseases in conjunction with functional abnormalities. However, their resolutions are limited due to the long acquisition time. Such datasets are multi-dimensional, exhibiting interactions between ≥ 4 dimensions, which cannot be easily identified using sparsity or low-rank matrix methods. Hence, low-rank tensors are a natural fit to model such data. But in the presence of multitude of different tissue types in the field-of-view, it is difficult to find an appropriate value of tensor rank, which avoids under- or over-regularization. In this work, we propose a locally low-rank tensor regularization approach to enable high-resolution quantitative dynamic MRI. We show this approach successfully enables dynamic T_1 mapping at high spatio-temporal resolutions.**

I. INTRODUCTION

Acquisition time in magnetic resonance imaging (MRI) still remains a challenge, often necessitating trade-offs between SNR, and spatial and temporal resolutions. Over the past decades, several methods have been proposed to improve resolution without sacrificing image quality or increasing scan time. Parallel imaging is the clinical gold standard for fast MRI, and relies on the redundancy among multiple-coil sensor/receive-arrays [1], [2]. Compressed sensing is an alternative technique that exploits the sparsity of the signal in a transform domain for regularized reconstruction from sub-sampled data [3], [4].

For scenarios where an image series is acquired, such as in dynamic MRI, this regularization can be extended to multi-way arrays to capture the multiple interactions between dimensions by exploiting inter-dimensional redundancies. For dynamic MRI, low-rank matrix regularization has been applied to exploit temporal redundancies, by vectorizing each image in the time-series [5], [6]. It has also been used in conjunction with other regularizers [7], [8]. To reduce the spatial blurring associated with the global low-rank processing, locally low-rank matrix regularization was proposed [9], [10]. Such regularized techniques have also been used for multiple-coil arrays [11], [12] or as post-processing after parallel imaging for reducing the effects of noise amplification [13], [14]. The advantage of the latter is that it requires no modification to existing clinical acquisition protocols, which typically acquire a uniformly sub-sampled Fourier space.

Over the past decade, there has been a push towards quantitative MRI, which provides characterization of the magnetization relaxation processes that are used to generate soft-tissue contrast [15]. This improves robustness and reproducibility, while enabling diagnosis of a broader class of diseases. However, it requires imaging the same anatomy with multiple different contrasts, leading to longer acquisition times. This challenge is more pronounced in a dynamic setting with moving structures (e.g. the beating heart). Such datasets are multi-dimensional, including spatial, contrast and time dimensions. Thus, they are better described with tensors than matrices, as analysis based on the latter is limited to pairwise interactions and may not show some hidden structures. The use of tensor methods has been limited in MRI [16], [17], and confined to global processing so far.

In this work, we sought to use low-rank tensor regularization on local patches to enable high-resolution quantitative dynamic cardiac MRI for joint evaluation of tissue viability and function. The proposed method is compared to a global tensor regularizaton approach, as well as parallel imaging. The performance improvement is evaluated in dynamic in-vivo myocardial parameter mapping, acquired at high spatial and temporal resolutions.

II. METHODS

A. Data Acquisition Model

In this study, a recently proposed MRI sequence [18] was used for dynamic (i.e., cardiac phase-resolved) quantification of the longitudinal relaxation (T_1) time, a biomarker with proven clinical utility in numerous cardiomyopathies [15]. The desired image data, $\mathbf{m}(x, y, t, c)$ is 4-dimensional, where (x, y) is the discrete 2D spatial location, t is the cardiac phase and c is different T_1 contrasts.

Acquired data in Fourier space (i.e., k-space) is given as

$$\mathbf{y}(t,c) = \mathbf{E}_{t,c}\big(\mathbf{m}(x,y,t,c)\big) + \mathbf{n}(t,c), \quad t = 1,\dots,T;\ c = 1,\dots,C \tag{1}$$

where $\mathbf{E}_{t,c} : \mathbb{C}^{M\times N} \rightarrow \mathbb{C}^P$ is the measurement system, including a partial Fourier matrix and the sensitivities of the receiver coil array, $\mathbf{n}(t,c) \in \mathbb{C}^P$ is measurement noise, t is the cardiac phase, c is the contrast-weighting, and x, y are the discrete spatial locations.

Once the image data $\mathbf{m}(x, y, t, c)$ is reconstructed from $\{\mathbf{y}(t,c)\}_{t,c}$, the underlying T_1 value is estimated for each (x, y, t) by a parameter estimation procedure across the contrast (c) dimension. The estimation is based on the Bloch equations describing the magnetization evolution [18].

Imaging was performed on a 3 Tesla scanner (Magnetom Prisma, Siemens Healthcare, Germany) using a 30-channel receiver coil-array. The MRI sequence parameters were chosen identical to [18], except for improved spatial and temporal resolutions (1.3×1.3 mm^2 spatial resolution and 40 ms

temporal resolution, instead of 2×2 mm^2 and 60 ms utilized in [18]). An acceleration rate of 3 was used with uniform sub-sampling to achieve this improved resolution, while decreasing the scan time to 18 seconds from 21 seconds achieved in [18]. 24 reference lines were acquired in the center of k-space to facilitate parallel imaging reconstruction. The dataset comprised $C = 5$ different contrast weightings and $T = 11$ cardiac phases.

B. Low-Rank Tensor Methods

The complex-valued 4D imaging dataset, $\mathbf{m}(x, y, t, c) \in \mathbb{C}^{M \times N \times T \times C}$ is represented as a fourth-order tensor

$$\mathbf{m} = \sum_{r=1}^{R} \mathbf{a}_r \circledcirc \mathbf{b}_r \circledcirc \mathbf{c}_r \circledcirc \mathbf{d}_r$$

$$\iff \mathbf{m}(i, j, k, l) = \sum_{r=1}^{R} \mathbf{a}_r(i)\mathbf{b}_r(j)\mathbf{c}_r(k)\mathbf{d}_r(l) \quad (2)$$

where $\circledcirc$ represents outer product and R represents the rank of tensor $\mathbf{m}$, the minimum number of rank-one tensors needed to synthesize $\mathbf{m}$ as their sum. Finding the rank of a tensor is an NP-hard problem, with an upper bound given by $\min\{MNT, MNC, MTC, NTC\}$ [19].

Tucker and PARAFAC decompositions are two main approaches in low-rank tensor approximation. PARAFAC decomposition method uniquely factorizes a tensor into a sum of rank-one tensors; whereas Tucker decomposition factorizes a tensor into a core tensor multiplied by a matrix along each mode. Previous works for tensor regularization have used both the Tucker [17] and PARAFAC [20] models. Of these two approaches, the Tucker model is typically used for compression applications [19], and in our context it requires choosing four mode ranks, as it assumes low-rank in each mode. PARAFAC is a direct low-rank decomposition that is mostly used for latent signal estimation, and uses a single tensor rank parameter. We adopt the latter in our work.

In previous applications of tensor regularization to MRI [17], [20], the regularization was performed globally. However, the imaging field-of-view contains multiple structures with different functional and contrast properties. For instance, the chest wall and back contain stationary tissue that is high in fat, which has a very short T_1 (< 250 ms). The heart muscle (myocardium) on the other hand contracts and expands substantially through the cardiac cycle and has a longer T_1 (≈ 1500 ms). The blood pools also move and have even longer T_1 (> 2000 ms). Thus, it is hard to capture all the information in a few rank-one components. Hence, in this work, we consider small local patches in the spatial domain and model these as low-rank tensors. This increases the likelihood that a patch contains only tissue types that are related in function and contrast, instead of a large number of tissue types with varying properties.

C. Tensor-Regularized Reconstruction

The sub-sampled data was reconstructed using parallel imaging reconstruction [2]. Parallel imaging was applied to each of $C = 5$ contrast weightings and $T = 11$ cardiac phases individually to avoid any temporal and/or contrast blurring in the reconstructed images. Tensor regularization was then used to reduce the noise amplification due to the linear parallel imaging reconstruction [1] in post-processing, similar to [13], [14]. The low-rank tensor factorization for noise reduction of a 4-dimensional noisy tensor $\mathbf{X}$ amounts to solving

$$\min_{\{\mathbf{a}_r, \mathbf{b}_r, \mathbf{c}_r, \mathbf{d}_r\}_{r=1}^{R}} \|\mathbf{X} - \sum_{r=1}^{R} \mathbf{a}_r \circledcirc \mathbf{b}_r \circledcirc \mathbf{c}_r \circledcirc \mathbf{d}_r\|_F^2 \quad (3)$$

Instead of solving the above least square problem which is non-convex, we use an alternating least squares (ALS) approach [19], [21]. ALS solves for $\{\mathbf{a}_r\}$ by fixing $\{\mathbf{b}_r\}$, $\{\mathbf{c}_r\}$ and $\{\mathbf{d}_r\}$ so that problem becomes (conditionally) linear. The procedure is then repeated for the other components until a stopping criterion is met.

Locally low-rank processing was implemented by extracting $8 \times 8 \times 11 \times 5$ patches from the imaging dataset, which were processed as 4-dimensional tensors. Overlapping patches were used with a shift of four, which were combined via averaging after processing. Ranks of $\{10, 20, 30, 40, 50, 100\}$ were used for approximation, with the upper bound on rank being 320. The locally low-rank tensor approach was compared to global tensor regularization applied to the 4-dimensional dataset. For the global tensor regularization, ranks of $\{100, 200, 300, 400, 500, 600\}$ were empirically investigated, with the rank upper bound being 7425.

D. Quantitative T_1 Map Analysis

The performance of the regularizations were evaluated using the quantitative T_1 maps. For each of the 11 cardiac phases, quantitative T_1 maps were generated. For each pixel in the T_1 map, the contrast changes across the 5 different T_1-weighted images were used to estimate the underlying T_1 parameter. This parameter estimation is possible, since the variations across the T_1 weighted images can be modeled using the Bloch equations as a function of T_1, as well as some of the acquisition parameters [18]. Once this processing is completed, for each imaging dataset, a 2D pixel-wise map of T_1 values has been generated, across each of the eleven cardiac phases. Since the T_1 values are in milliseconds, this allows for a quantitative characterization of the regularization performance.

Myocardial (heart muscle) T_1 times are the quantity of interest for evaluation of various cardiac diseases [15]. Thus, regions-of-interest (ROIs) were manually drawn in the myocardium, for each of the cardiac phases. The mean value in the ROI is recorded as the estimate of the myocardial T_1 value. The standard deviation in the ROI is recorded as the spatial variability, which is used as a surrogate for precision. The T_1 times and the precision were averaged across all cardiac phases (as mean $\pm$ standard deviation), to give a metric for estimated T_1, as well as overall precision.

There are two components to the evaluation of the regularization: 1) The method should be unbiased, i.e. the average T_1 value estimated by the method should not be altered due to regularization; 2) The method should improve precision, i.e. the noise amplification in the dataset, and therefore the spatial variability in the T_1 maps should be reduced as much as possible with the regularization. Both quantities were used to evaluate the performance of the global and the proposed local low-rank tensor regularizations.

III. RESULTS

A. *Effect of Tensor Rank*

Figure 1a depicts T_1 maps from a representative cardiac phase, out of the eleven acquired ones for global (top) and local (bottom) low-rank tensor (LRT) regularization, with different tensor ranks. The maps are zoomed into the heart for better visibility and the myocardial muscle is in the green-like color. Global LRT regularization exhibits spatial blurring artifacts, as depicted in the blood-myocardium border, for low ranks (e.g. 100). With increasing rank, the spatial blurring is ameliorated, but the dataset gets noisier. The proposed local LRT regularization does not suffer from similar blurring artifacts at the lowest ranks, due to more localized features that are picked up in these small patches. As expected, noisier maps are observed with increasing rank in this case as well.

Figure 1b depicts the quantitative metrics for precision and T_1 time estimates, which confirm the behavior observed in (a). For both LRT regularizations, the average precision degrades with increasing rank (top). Both the best precision and the best standard deviation of precision across cardiac cycles are achieved with the lowest ranks that were investigated for both methods. In terms of the estimated T_1 values (bottom), the proposed locally LRT regularization is unbiased across the ranks that were investigated. However, the global LRT approach shows biased T_1 times for small ranks, in the range of 100-400. This is possibly a by-product of the spatial blurring observed in Figure 1a, biasing the myocardial T_1 times towards the higher blood T_1 times.

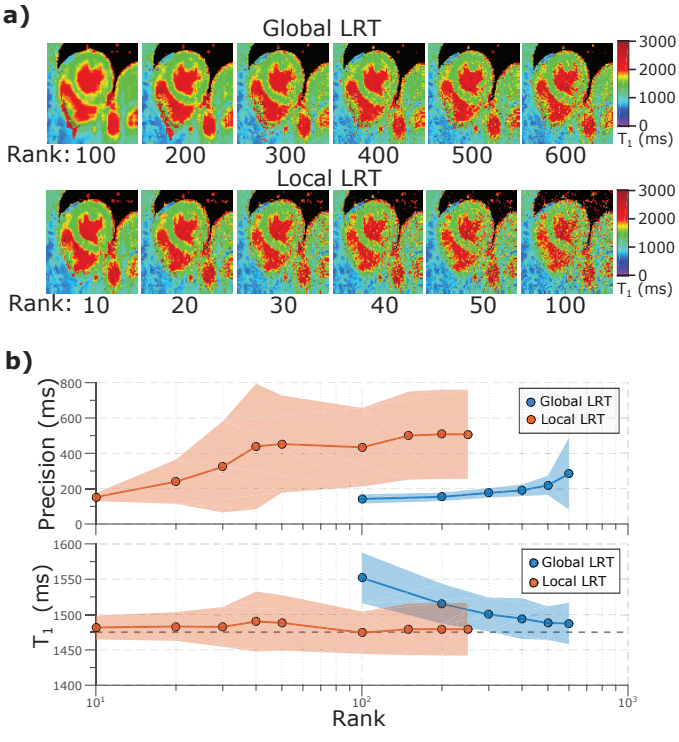

Fig. 1. a) T_1 maps of a representative cardiac phase (zoomed into heart) for global (top) and local (bottom) low-rank tensor (LRT) regularization, for various ranks. Global LRT exhibits blurring artifacts for low ranks, and more noise for higher ranks. Local LRT does not suffer from spatial blurring at low ranks. b) The quantitative metrics confirm the behavior in (a), with precision degrading with increasing rank (top); and global LRT exhibiting bias in T_1 value estimation at the lower ranks (bottom).

Based on these experiments, ranks of 10 and 500 were chosen for the local and global LRT regularization schemes for the remainder of the text, as these provide the best improvements in precision without biasing the estimated quantitative values.

B. *Improved High-Resolution Dynamic T_1 Maps*

Figure 2 depicts the dynamic quantitative T_1 maps of all cardiac phases in a healthy volunteer. Major noise variations are readily observed in the baseline images, generated using parallel imaging (top). Due to the high-resolution of the acquisitions, the SNR of the acquisition is low, and noise amplification of parallel imaging [1] renders these maps clinically unusable. This is further evidenced by the quantitative characterization of precision across all cardiac phases, which is 336 ± 39 ms, leading to a spatial variability of $\approx 25\%$ of the T_1 value. The noise degradation is especially apparent in the later cardiac phases, due to less magnetization changes for the T_1 parameter estimation [18].

Global LRT regularization, with rank 500, significantly improves the visual quality of the dynamic T_1 maps (middle). There are some residual artifacts, such as signal contamination from the blood pool in the earlier phases, as well as residual inhomogeneity in the myocardium in the later cardiac phases. The overall precision for this technique is 219 ± 54 ms. The proposed local LRT regularization, with rank 10, further suppresses these artifacts, while preserving the contrast variation and the sharp border delineation between the blood and the myocardium. The noise reduction is also more uniform across the cardiac phases, with late cardiac phases exhibiting limited noise amplification in the myocardium. The overall precision for this technique is 153 ± 23 ms. Thus, the proposed approach outperforms global LRT regularization both visually and quantitatively; and improves upon the precision of parallel imaging by more than a factor of 2.

Figure 3 depicts the T_1 values through the cardiac phases for a cross-section of the heart. This helps to capture the functional information assessed from the dynamic nature of the acquisition. Functional representation of cardiac motion is deteriorated in parallel imaging due to the high noise amplification, which makes it difficult to identify tissue borders. Both global and local LRT approaches significantly decrease these noise artifacts, while preserving the dynamic profile across the cardiac cycle.

IV. DISCUSSION AND CONCLUSIONS

In this study, we proposed locally low-rank tensor regularization approach for MRI reconstruction, and applied it to a high-resolution dynamic cardiac T_1 mapping acquisition [18]. The method was compared to conventional parallel imaging, as well as global low-rank tensor regularization, and was shown to be superior to both, visually and quantitatively.

The proposed regularization in conjunction with the accelerated acquisition considered here enables T_1 mapping with a spatial resolution of 1.3×1.3 mm^2 and temporal resolution of 40 ms. Conventional T_1 mapping acquisitions are confined to spatial resolutions of 2×2 mm^2 and temporal resolution of 200-250 ms [15]. These improvements may facilitate better delineation of blood-myocardium border, thereby reducing

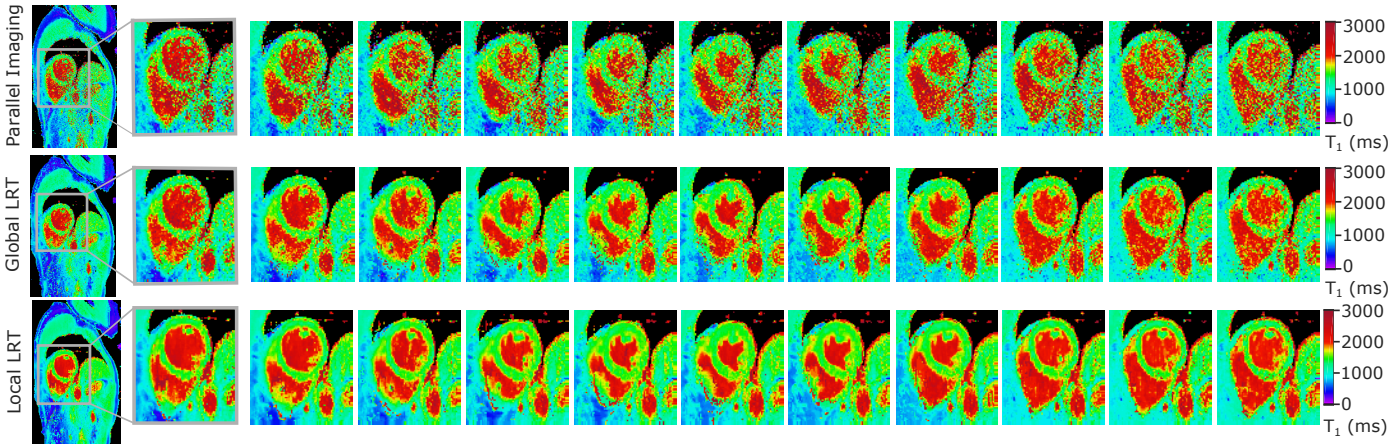

Fig. 2. Dynamic quantitative T_1 maps generated with conventional parallel imaging (top), global LRT (middle) and the proposed local LRT (bottom). The full field-of-view are images depicted on the left for one cardiac phase; and the T_1 maps for all eleven cardiac phases are shown. The local LRT approach significantly reduces the noise inhomogeneity of parallel imaging, and eliminates the residual noise artifacts present in the global LRT approach. Overall spatial variability of the myocardial T_1 values for the three methods are 336 ± 39 ms, 219 ± 54 ms, and 153 ± 23 ms, respectively, showing a significant improvement with the proposed regularization.

partial voluming artifacts; as well as characterization of smaller highly mobile structures, such as the papillary muscles.

The datasets acquired in this study are 4-dimensional, containing two spatial dimensions, one dimension for cardiac motion, and a dimension along which the contrast weighting of images changes based on T_1. There are multiple interactions among these dimensions, which cannot be captured efficiently in a pair-wise manner. Thus, while low-rank matrix regularization has been employed in MRI [6], [8], [9], low-rank tensors are a natural fit to represent this dynamic myocardial T_1 mapping data. Additionally since the imaging field-of-view contains multiple structures with different functional and contrast properties (e.g. the full field-of-view image in Figure 2), local use of the tensor properties proved to be beneficial in improving both the visual image quality and the quantitative metrics for precision.

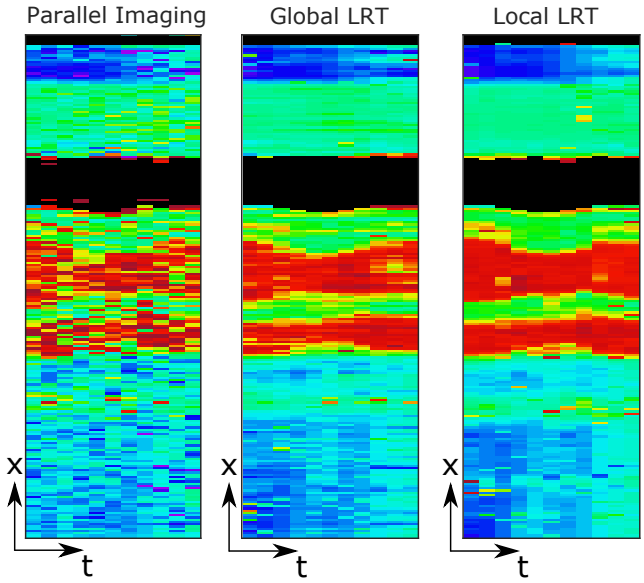

Fig. 3. T_1 times through cardiac phases across a cross-section of the heart. Parallel imaging suffers from noise amplification, making it difficult to identify tissue borders. The tensor-regularized methods significantly decrease these noise artifacts, while showing no temporal blurring across the cardiac cycle.

Both Tucker and PARAFAC decompositions have been used in MRI for regularization [17], [20]. The former is a form of higher order singular value decomposition. Tucker-based low-rank tensor approach gathers the highest energy slabs for each mode in a part of the core, then truncates the core. However, such truncation does not necessarily yield a good approximation for the tensor [19], since there is no tensor equivalent form of the Eckart-Young theorem which gives the best low-rank matrix approximation by keeping a few large singular values and truncating the rest of the singular values. PARAFAC model has a direct relationship with the rank and by extension with low-rank approximation, since it is the summation of rank-one tensors. Furthermore, since PARAFAC decomposition uses fewer degrees of freedom than Tucker, it is less susceptible to over-fitting, avoiding excessive modeling of noise and other system imperfections [22].

In addition to the imaging performance improvements, the proposed locally low-rank tensor model also has a computational advantage over the globally low-rank tensor regularization, due to the considerably reduced rank. This translates to a 10-fold improvement in computational time. Note the processing time could be further reduced using parallelization on multi-cores or GPUs, but this was not investigated in the current study.

A single rank was used to process all 4-dimensional patches in the dataset. An adaptive rank selection may be desirable to further increase the noise reduction quality, but this was not explored. In this work, the regularization was applied to images reconstructed with parallel imaging, which resulted in no iterative processing.

ACKNOWLEDGMENT

This work was partially supported by NIH R00HL111410, NIH P41EB015894, NSF CCF-1651825 and NSF IIS-1704074

REFERENCES

[1] K. P. Pruessmann, M. Weiger, M. B. Scheidegger and P. Boesiger, "SENSE: sensitivity encoding for fast MRI," *Magn. Reson. Med.*, vol. 42, no. 5, pp. 952-962, 1999.

[2] M. A. Griswold, P. M. Jakob, R. M. Heidemann, M. Nittka, V. Jellus, J. Wang, B. Kiefer and A. Haase, "Generalized autocalibrating partially parallel acquisitions (GRAPPA)," *Magn. Reson. Med.*, vol. 47, no. 6, pp. 1202-1210, 2002.

[3] M. Lustig, D. Donoho and J. M. Pauly, "Sparse MRI: The application of compressed sensing for rapid MR imaging," *Magn. Reson. Med.*, vol. 58, no. 6, pp. 1182-1195, 2007.

[4] K. T. Block, M. Uecker and J. Frahm "Undersampled radial MRI with multiple coils: Iterative image reconstruction using a total variation constraint," *Magn. Reson. Med.*, vol. 57, no. 6, pp. 1086-1098, 2007.

[5] B. Zhao, J. P. Haldar, A. G. Christodoulou and Z. P. Liang, "Image reconstruction from highly undersampled (k,t)-space data with joint partial separability and sparsity constraints," *IEEE Trans. Med. Imag.*, vol. 31, no. 9, pp. 1809-1820, 2012.

[6] J. P. Haldar and Z. P. Liang,"Low-rank approximations for dynamic imaging," in *Proc. IEEE Int. Symp. Biomed. Imag.*, pp. 1052-1055, 2011.

[7] R. Otazo, E. Cands and D. K. Sodickson, "Low-rank plus sparse matrix decomposition for accelerated dynamic MRI with separation of background and dynamic components," *Magn. Reson. Med.*, vol. 73, no. 3, pp. 1125-1136, 2015.

[8] S. G. Lingala, Y. Hu, E. DiBella and M. Jacob , "Accelerated dynamic MRI exploiting sparsity and low-rank structure: k-t SLR," *IEEE Trans. Med. Imag.*, vol. 30, no. 5, pp. 1042-1054, 2011.

[9] J. D. Trzasko, A. Manduca and E. Borisch, "Local versus global low-rank promotion in dynamic MRI series reconstruction," in *Proc. Int. Soc. Magn. Reson. Med.*, p. 4371, 2011.

[10] T. Zhang, J. M. Pauly and I. R. Levesque, "Accelerating parameter mapping with a locally low-rank constraint," *Magn. Reson. Med.*, vol. 73, no. 2, pp. 655-661, 2015.

[11] P. J. Shin, P. E. Larson, M. A. Ohliger, M. Elad, J. M. Pauly, D. B. Vigneron and M. Lustig, "Calibrationless parallel imaging reconstruction based on structured low rank matrix completion," *Magn. Reson. Med.*, vol. 72, no. 4, pp. 959-970, 2014.

[12] J. P. Haldar and J. Zhuo, "P-LORAKS: Low rank modeling of local kspace neighborhoods with parallel imaging data," *Magn. Reson. Med.*, vol. 75, no. 4, pp. 1499-1514, 2016.

[13] J. Veraart, D. S. Novikov, D. Christiaens, B. Ades-Aron, J. Sijbers and E. Fieremans, "Denoising of diffusion MRI using random matrix theory," *Neuroimage*, vol. 142, pp. 394-406, 2016.

[14] J. V. Manjon, P. Coupe, L. Concha, A. Buades, D. L. Collins and M. Robles, "Diffusion Weighted Image Denoising Using Overcomplete Local PCA," *PLoS ONE*, vol. 8, no. 9, 2013.

[15] E. B. Schelbert and D. R. Messroghli DR, "State of the art: clinical applications of cardiac T_1 mapping," *Radiology*, vol. 278, pp. 658-676, 2016.

[16] J. D. Trzasko and A. Manduca, "A unified tensor regression framework for calibrationless dynamic, multi-channel MRI reconstruction," in *Proc. Int. Soc. Magn. Reson. Med.*, p. 603, 2013.

[17] J. He, Q. Liu, A. G. Christodoulou, C. Ma, F. Lam and Z. P. Liang, "Accelerated high-dimensional MR imaging with sparse sampling using low-rank tensors," *IEEE Trans. Med. Imaging*, vol. 35, no. 9, pp. 2119-2129, 2016.

[18] S. Weingartner, C. Shenoy, B. Rieger, L. R. Schad, J. Schulz-Menger and M. Akçakaya, "Temporally resolved parametric assessment of Z-magnetization recovery (TOPAZ): Dynamic myocardial T1 mapping using a cine steady-state look-locker approach," *Magn. Reson. Med.*, doi:10.1002/mrm.26887, 2017.

[19] N. D. Sidiropoulos, L. De Lathauwer, X. Fu, K. Huang, E. E. Papalexakis and C. Faloutsos, "Tensor decomposition for signal processing and machine learning," *IEEE Trans. Signal Processing*, vol. 65, no. 13, pp. 3551-3582, 2017.

[20] N. Kargas, S. Weingartner, N. D. Sidiropoulos and M. Akçakaya, "Low-rank tensor regularization for improved dynamic quantitative magnetic resonance imaging," *SPARS*, 2017.

[21] T. G. Kolda and B. W. Bader, "Tensor decompositions and applications," *SIAM Rev.*, vol. 51, no. 3, pp. 455-500, 2009.

[22] R. Bro, "PARAFAC. Tutorial and applications," *Chemometr. Intell. Lab. Syst.*, vol. 38, no. 2, pp. 149-171, 1997.